Journal of Magnetic Resonance 231 (2013) 133–140

Contents lists available at SciVerse ScienceDirect

Journal of Magnetic Resonance

journal homepage: www.elsevier.com/locate/jmr

Room temperature strong coupling between a microwave oscillator and an ensemble of electron spins

G. Boero [a,*], G. Gualco [a], R. Lisowski [a], J. Anders [a,c], D. Suter [b], J. Brugger [a]

[a] Ecole Polytechnique Federale de Lausanne (EPFL), CH-1015 Lausanne, Switzerland
[b] Technische Universität Dortmund, D-44221 Dortmund, Germany
[c] Universität Ulm, D-89069 Ulm, Germany

ARTICLE INFO

Article history:
Received 27 February 2013
Revised 5 April 2013
Available online 18 April 2013

Keywords:
EPR
Strong coupling
LC-oscillator

ABSTRACT

We demonstrate theoretically and experimentally the possibility to achieve the strong coupling regime at room temperature with a microwave electronic oscillator coupled with an ensemble of electron spins. The coupled system shows bistable behaviour, with a broad hysteresis and sharp transitions. The coupling strength and the hysteresis width can be adjusted through the number of spins in the ensemble, the temperature, and the microwave field strength.

1. Introduction

Achieving strong coupling between a microwave resonator and an ensemble of electron spins has become an important goal during the last years [1–14]. One of the motivations for these studies is the search for possible realizations of efficient quantum computers. The strength of the coupling between a resonator and an ensemble of electron spins is usually described by the collective coupling strength [2–5]. The collective coupling strength g_c can be expressed as $g_c = g_s\sqrt{N_p}$, where g_s is the cavity-single spin coupling strength, $N_p = N(\coth(\alpha) - (1/\alpha))$ is the equivalent number of polarized spins, $\alpha = \mu B_0/k_B T$, μ is the effective magnetic moment ($\mu = \mu_B\sqrt{3}$ for $S = 1/2$ and $g = 2$), B_0 is the static magnetic field, and N is the number of spins in the ensemble. A rough estimation of g_s is given by $g_s \cong \mu\sqrt{\mu_0\omega/2\hbar V_c}$ where V_c is the cavity volume, and ω is the transition angular frequency [2]. The strong coupling regime is usually identified by the conditions $g_c \gg \kappa, \gamma$, where κ and γ are the resonator and the spin resonance line half-width-at-half-maximum, both given in rad/s [2,4,5].

In contrast to previous work that described the coupling between a microwave *resonator* driven by an external microwave source and a spin ensemble [1–9,15,16], here we investigate theoretically and experimentally the coupling of a microwave *oscillator* and an ensemble of spins. In particular, we provide a simple theory describing the coupling of a microwave LC-oscillator with an ensemble of electron spins and we demonstrate experimentally that by this approach the strong coupling is observable also at room temperature. The strong coupling between the spin ensemble and the microwave oscillator leads to a cooperative behaviour of the combined system. The oscillation frequency of the coupled system shows a broad hysteresis and sharp transitions as a function of the applied static magnetic field. In the bistable region, the previous history of the system determines which of the two possible states is observed.

2. Theory

In typical experimental conditions, the oscillation frequency of an LC-oscillator coupled with an ensemble of electron spins is given by (see Appendix A)

$$\omega_{LC\chi} \cong \frac{\omega_{LC}}{\sqrt{1+\eta\chi'}}, \tag{1}$$

where

$$\chi' = -\frac{1}{2}\frac{(\omega_{LC\chi}-\omega_0)T_2^2}{1+T_2^2(\omega_{LC\chi}-\omega_0)^2+\gamma_e^2 B_1^2 T_1 T_2}\omega_0\chi_0, \tag{2}$$

$\omega_{LC} = 1/\sqrt{LC}$ is the unperturbed oscillator frequency, $\omega_0 = \gamma_e B_0$, χ_0 is the static susceptibility, η is the filling factor (approximately given by (V_s/V_c), where V_s is the sample volume), γ_e is the electron gyromagnetic ratio, B_1 is the microwave magnetic field, T_1 and T_2 are the relaxation times. Due to the dependence of χ' on $\omega_{LC\chi}$, Eq. (1) contains on both sides the oscillation frequency $\omega_{LC\chi}$. The determination of $\omega_{LC\chi}$ is equivalent to the determination of the roots of the function $F(\omega_{LC\chi}, B_0) = \omega_{LC\chi} - (\omega_{LC}/\sqrt{1+\eta\chi'})$ (or to the

* Corresponding author. Address: Ecole Polytechnique Fédérale de Lausanne (EPFL), BM-3-110, Station 17, CH-1015 Lausanne, Switzerland.
E-mail address: giovanni.boero@epfl.ch (G. Boero).

1090-7807/$ - see front matter
http://dx.doi.org/10.1016/j.jmr.2013.04.004

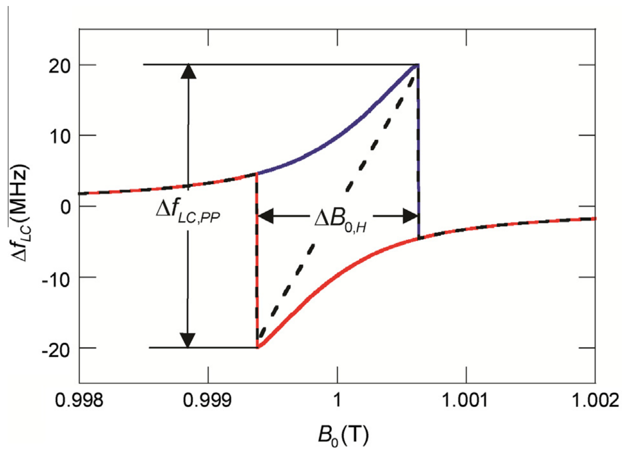

Fig. 1. Graphical representation of the three solutions for the oscillator frequency variation $\Delta f_{LC} = (\omega_{LC\chi} - \omega_{LC})/2\pi$ obtained solving Eq. (1). Simulation parameters: $T_1 = T_2 = 60$ ns, $\chi_0 = 5.2 \times 10^{-5}$, $f_{LC} = 28$ GHz, $\gamma_e/2\pi = 28$ GHz/T, $\eta = 0.01$, $B_1 = 0$. The static susceptibility is computed by the equation $\chi_0 = \mu_0 n \gamma_e^2 \hbar^2/4kT$ (which is valid for $S = 1/2$, $g = 2$, $\mu B_0 \ll kT$) assuming $T = 300$ K and $n = 2 \times 10^{27}$ spins/m^3. Relaxation times and spin density correspond to those of DPPH [17,18]. $\Delta f_{LC,PP}$ is the peak-to-peak oscillator frequency variation, $\Delta B_{0,H}$ is the hysteresis.

determination of the extrema of $U(\omega_{LC\chi}, B_0) = -\int F(\omega_{LC\chi}, B_0) d\omega_{LC\chi}$, which assumes the role of a pseudo potential).

We first discuss the solution of Eq. (1) in the limit of negligible saturation (i.e., for $\gamma_e^2 B_1^2 T_1 T_2 \ll 1$). As long as the coupling is weak (precisely for $(\eta\chi_0)^{1/2} T_2 \omega_0 < 2$), there is a single solution for $\omega_{LC\chi}$ for each value of B_0. For $(\eta\chi_0)^{1/2} T_2 \omega_0 \geqslant 2$, we find a single solution *far* from resonance and three solutions *close* to resonance. The condition $(\eta\chi_0)^{1/2} T_2 \omega_0 \geqslant 2$ is equivalent to the strong coupling condition $g_c \geqslant \gamma$ (see Appendix B). Fig. 1 shows an example of the solutions obtained in the conditions reported in the figure caption, which correspond to $(\eta\chi_0)^{1/2} T_2 \omega_0 \cong 8$. The curve plotted in blue corresponds to the curve experimentally observed when the magnetic field is swept from values well below resonance to higher values, whereas the curve in red[1] corresponds to the opposite sweep direction starting from a field value well above resonance. Due to the hysteresis, a sort of volatile memory is obtained. The solution plotted with a dashed line in black is not experimentally observed. This solution corresponds to a maximum of the pseudo potential U and it is given by $\omega_{LC\chi} = \omega_0$ within the hysteresis. If the oscillator is turned on with a magnetic field value within the hysteresis region, the solution in red is experimentally observed. This might be due to the relatively complex start-up mechanisms of the oscillations or to a not yet identified global energy minimum of the system (the pseudo potential has two local minima with the same pseudo energy).

The physical behaviour of the LC-oscillator coupled to the spin ensemble can be qualitatively explained as follows. If the field sweep is started from a field value below (above) the resonance conditions, the oscillator frequency $\omega_{LC\chi}$ is slightly above (below) the unloaded oscillator frequency ω_{LC} due to the negative (positive) susceptibility χ' (see Eq. (1)). If the magnetic field is swept towards higher (lower) values the oscillator frequency $\omega_{LC\chi}$ further increases (decreases) due to the change of the susceptibility. This is the reason why sweeping the field towards higher (lower) values the resonance condition is achieved for a field $B_0 \geqslant (\omega_{LC}/\gamma_e)$ ($B_0 \leqslant (\omega_{LC}/\gamma_e)$). The oscillator remains locked to the spin system even when the magnetic field has been increased (decreased) beyond the resonance condition for the uncoupled system $B_0 = (\omega_{LC}/\gamma_e)$.

[1] For interpretation of colour in Fig. 1, the reader is referred to the web version of this article.

Fig. 2a–d show the evolution of the oscillator frequency variation as a function of the static magnetic field for different values of the filling factor. For $\eta = 0.0001$ the frequency variation has a dispersion-like shape. For $\eta \geqslant 0.001$, which corresponds to $(\eta\chi_0)^{1/2} T_2 \omega_0 \geqslant 2$, a hysteresis together with sharp transitions appears. The abrupt frequency variations shown in Fig. 2b–d are infinitely sharp (i.e., a forbidden frequency band exists between the two allowed frequency values immediately before and after the transition). Fig. 2e shows the linear dependence of the oscillator frequency variation $\Delta f_{LC,PP}$ on the filling factor. The oscillator frequency variation is equal to $(1/8\pi)\omega_0^2 T_2 \eta \chi_0$, in the weak as well as in the strong coupling regime. Fig. 2e shows also that, for sufficiently large η, the width of the hysteresis $\Delta B_{0,H}$ is a linear function of the filling factor. For wide hystereses, the hysteresis width and the frequency variation are related by $\Delta B_{0,H} \cong \gamma_e 2\pi \Delta f_{LC,PP}$. Fig. 2f shows the slope of the oscillator frequency variation at resonance as a function of the filling factor. For small values of η, the slope grows linearly with the filling factor. Close to the onset of the hysteretic behaviour, the slope becomes orders of magnitude larger than the one predicted using a linear extrapolation from the slope at small filling factors. Fig. 2f shows also the field difference $\Delta B_{0,PP}$ between the extrema of the oscillator frequency variation. In the weak coupling limit, $\Delta B_{0,PP}$ corresponds to the resonance linewidth definition for a dispersion signal. In the strong coupling regime, $\Delta B_{0,PP} = \Delta B_{0,H}$. For η values just below the onset of the hysteresis, the dispersion signal is distorted and narrowed ($\Delta B_{0,PP}$ is reduced to half of its value in the weak coupling limit).

So far, we assumed negligible saturation of the spin system. Fig. 2g shows the oscillator frequency variation and the hysteresis width as a function of the microwave field strength. In the condition of negligible saturation, the oscillator frequency variation and the hysteresis width are approximately independent of B_1. In the condition of non-negligible saturation, the oscillator frequency variation as well as the hysteresis width decrease rapidly to zero.

3. Experiments

In order to experimentally verify the proposed simple theoretical model, we used a single-chip electron spin resonance detector similar to those we reported in [19,20]. Fig. 3 shows a photo and the block diagram of the realized chip, which essentially consists of two LC-oscillators operating at 20.6 GHz and 17.1 GHz, respectively. The excitation/detection octagonal coils have a diameter of 200 μm, an inductance of 300 pH, a resistance of 2 Ω, and a Q-factor of 20. The microwave magnetic field B_1 can be varied from 0.1 to 0.7 mT by changing the oscillator supply voltage from 0.5 to 3.5 V. On the same chip, a mixer and a frequency division stage are also integrated. By mixing the two oscillator output voltages a signal at about 3.5 GHz is obtained, which is subsequently divided by 16, resulting in a chip output signal at about 220 MHz. The output frequency is measured with a frequency counter as a function of the applied static magnetic field B_0. The experimental oscillator linewidth is $\kappa \cong 2 \times 10^4$ rad/s, as measured by the virtual damping rate method [21]. Due to a relatively large $1/f^3$ component in the oscillator phase noise [22], the measured κ is two orders of magnitude larger than the thermal noise limited value, with an experimental linewidth compression of about 5×10^{-6} (see Appendix C).

The experiments reported in Fig. 4 are performed with a sample of DPPH having a volume of about $90 \times 90 \times 50$ μm^3 and $T_2 \cong 56$ ns at 300 K as well as 77 K (see Appendix D). At 300 K, from the description of our experimental conditions reported above, we have $g_c \cong 2 \times 10^8$ rad/s, $\gamma \cong 2 \times 10^7$ rad/s, and $\kappa \cong 2 \times 10^4$ rad/s. Consequently, the strong coupling conditions $g_c \gg \gamma, \kappa$ are fulfilled. Fig. 4a reports measurements performed to experimentally dem-

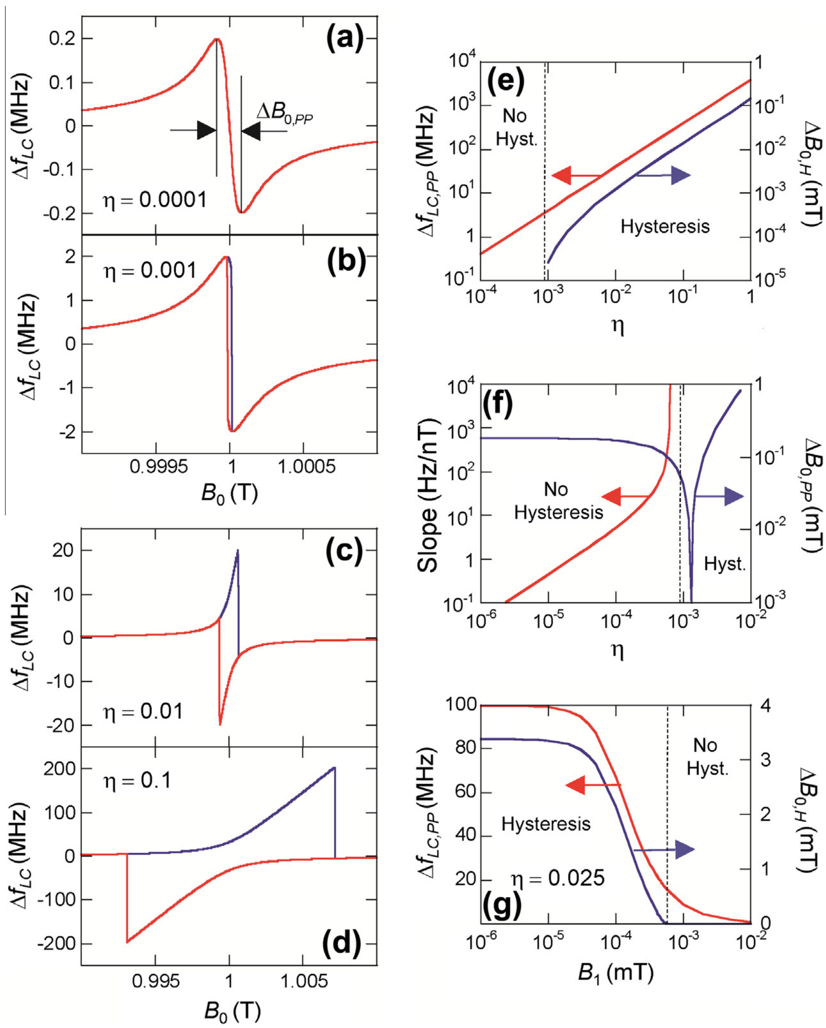

Fig. 2. (a–d) Oscillator frequency variation as a function of static magnetic field for different values of the filling factor for $B_1 = 0$. (a) $\eta = 0.0001$, (b) $\eta = 0.001$, (c) $\eta = 0.01$, (d) $\eta = 0.1$. (e) Oscillator frequency variation and hysteresis width as a function of the filling factor η for $B_1 = 0$. (f) Slope of the oscillator frequency variation at resonance (i.e., $[d(\Delta f_{LC})/dB_0]_{B_0=\omega_{LC}/\gamma_e}$) and resonance width $\Delta B_{0,PP}$ as a function of η for $B_1 = 0$. (g) Oscillator frequency variation and hysteresis width as a function of B_1 for $\eta = 0.025$. Simulations parameters: $T_1 = T_2 = 60$ ns, $\chi_0 = 5.2 \times 10^{-5}$, $f_{LC} = 28$ GHz, $\gamma_e/2\pi = 28$ GHz/T.

onstrate the possibility to achieve the strong coupling regime at room temperature. Fig. 4b reports measurements performed at 77 K with the same sample. Due to the enhanced spin polarization (i.e., larger static susceptibility χ_0) the oscillator frequency variation and hysteresis width at 77 K are about a factor of three to four larger than those at 300 K. Fig. 4c shows a narrow field sweep in correspondence with the sharp transition at higher fields. The transition is narrower than 20 nT, the smallest field variation possible with our set-up. The standard deviation of the *jitter* in the position of the sharp transitions is of about 1 μT in a measuring time of 30 min with 400 passages through the sharp transitions. This jitter is mainly due to the frequency noise of our integrated oscillator. As shown in Fig. 4d, the experimental results for the oscillator frequency variation and the hysteresis width are up to a factor four smaller than the values obtained by solving Eq. (1). The difference between the experimental and simulated results is probably due to the uncertainty on the values of T_1, B_1, spin density, and sample volume (see Appendix E).

Fig. 5 reports experiments performed at 300 K with a sample of BDPA having a volume of about $60 \times 70 \times 30$ μm^3 and $T_1 \cong T_2 \cong 100$ ns (see Appendix D). The strong coupling conditions are fulfilled also with this sample. Fig. 5a shows that the oscillator frequency variation as well as the hysteresis width decreases by increasing B_1. For B_1 values larger than 0.6 mT, the hysteresis disappears. Fig. 5b compares the theoretical and experimental values for the oscillator frequency variation and hysteresis width as a function of B_1. Fig. 6a reports experiments performed with samples of BDPA having three different volumes ($60 \times 70 \times 30$ μm^3, $60 \times 25 \times 30$ μm^3, $30 \times 20 \times 20$ μm^3), corresponding to three different filling factors η (0.018, 0.0064, 0.0017). Fig. 6b compares the theoretical and experimental values for the oscillator frequency variation and hysteresis width as a function of the filling factor. As in the case of DPPH, also with BDPA the agreement between experiments and simulations is within a factor of four. For both samples the agreement is worse for large values of the hysteresis.

4. Conclusion and outlook

In this work we have investigated theoretically and experimentally the strong coupling regime between an ensemble of electron spins and an electronic microwave oscillator. The system shows several interesting phenomena, such as bistability and hysteresis as a function of the applied static magnetic field. The proposed simple theoretical model explains the observed phenomena, at least at a semi-quantitative level.

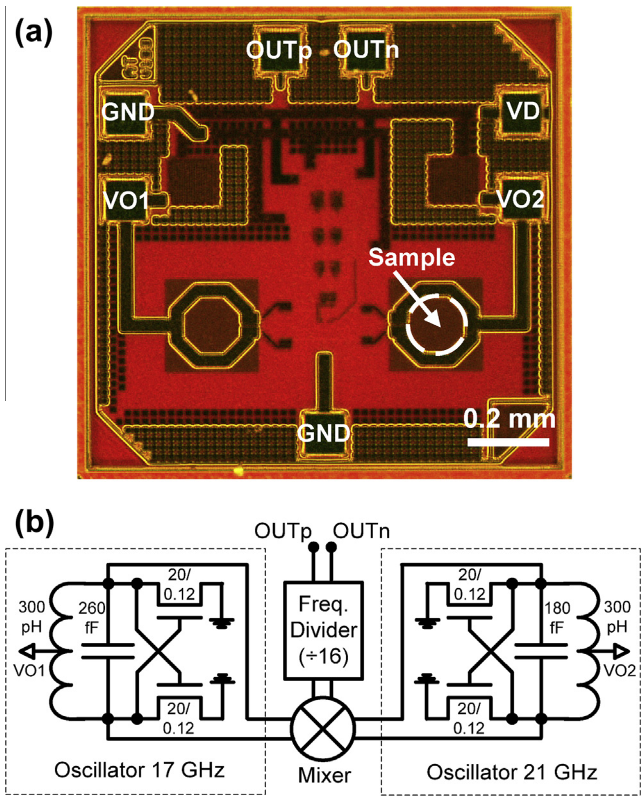

Fig. 3. (a) Optical microscope image and (b) block diagram of the single-chip electron spin resonance detector. VO1 and VO2: DC power supply of the two oscillators (0.5–3.5 V). VD: DC power supply for the mixer and frequency-division module (1.5 V). OUTp and OUTn: differential output signal (≅220 MHz). The transistor dimensions width/length are in micrometres. The dashed circle indicates the area where the samples are placed.

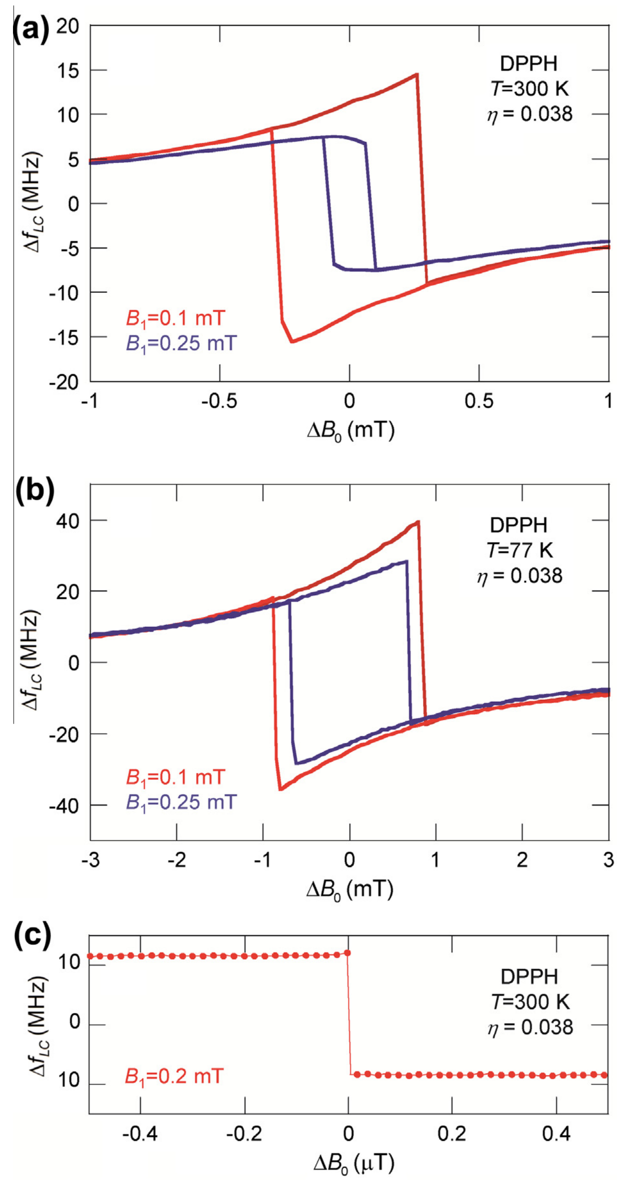

(d)

T (K)	B_1 (mT)	Exper. $\Delta f_{LC,PP}$ (MHz)	Simul. $\Delta f_{LC,PP}$ (MHz)	Exper. $\Delta B_{0,H}$ (mT)	Simul. $\Delta B_{0,H}$ (mT)
300	0.1	30	62	0.57	1.9
300	0.25	15	27	0.16	0.55
77	0.1	76	201	1.7	6.8
77	0.25	56	100	1.4	3.1

Fig. 4. Experimental oscillator frequency variation as a function of the static magnetic field for different values of B_1 with a DPPH sample of about $90 \times 90 \times 50\ \mu m^3$. (a) $T = 300$ K, $f_{LC} \cong 20.61$ GHz, $B_0 \cong 0.736$ T (for $\Delta B_0 = 0$). (b) $T = 77$ K, $f_{LC} \cong 20.89$ GHz, $B_0 \cong 0.746$ T (for $\Delta B_0 = 0$). (c) Narrow field sweep across one of the sharp transitions at $T = 300$ K, $f_{LC} = 20.61$ GHz, $B_1 \cong 0.2$ mT, $B_0 \cong 0.736$ T (for $\Delta B_0 = 0$). (d) Comparison between experiments and simulations (simulation parameters: $T_1 = T_2 = 60$ ns, $n = 2 \times 10^{27}$ spins/m^3, $\eta = 0.038$, $\gamma_e/2\pi = 28$ GHz/T).

In addition to the conceptually novel way in which the strong coupling regime with an ensemble of spins is revealed and manifests itself, the oscillator approach proposed here might have fundamental and practical advantages with respect to the resonator approach reported previously. Due to linewidth compression (see Appendix C), the linewidth of an oscillator is several orders of magnitude narrower compared to that of a passive resonator. This allows to achieve strong coupling at higher temperatures or with smaller or more diluted spin ensembles. Diluted spin ensembles have typically longer coherence times and well resolved line splitting thus allowing for more complex coherent spin manipulations [10,14]. The oscillator approach, combined with its implementation using advanced integrated circuit technologies as demonstrated in this paper, has the practical advantage of having the entire sensitive part of the excitation/detection chain integrated into a single chip, thus requiring no external microwave electronics. Consequently, the oscillator approach is well suited for the realization of dense arrays of highly miniaturized oscillator–spin ensemble systems on the same chip, potentially capable to simultaneously manipulate and read all spin ensembles in a correlated or independent fashion. The long spin coherence times recently reported for donors in ^{28}Si crystals [23,24] suggests a possible route for all-silicon large-scale spin-based quantum processing [25].

As mentioned in the introduction, the collective coupling strength g_c is proportional to $\sqrt{N_p/V_c}$. Consequently, the strong coupling for a given number of spins is more easily achievable with a miniaturized coil having a small sensitive volume V_c. In Refs. [19,20], we derived an approximate expression for the minimum number of spins which are detectable inductively. Assuming $T = 1$ K, $T_1 = T_2 = 10\ \mu s$, $R = 1\ \Omega$, $f_{LC} = 280$ GHz, $B_u = 0.13$ T/A (i.e., a single turn coil with a diameter of 10 μm), and $\kappa \cong 10^4$ rad/s, we obtain $N_{min} \cong 1$ spin/Hz$^{1/2}$, $\gamma \cong 10^5$ rad/s, and, for a single spin, $g_c \cong 10^5$ rad/s. Under these assumptions (see discussion in Appendix E) the spin sensitivity and the coupling parameters are at the limit of allowing the detection of a single spin in the strong coupling

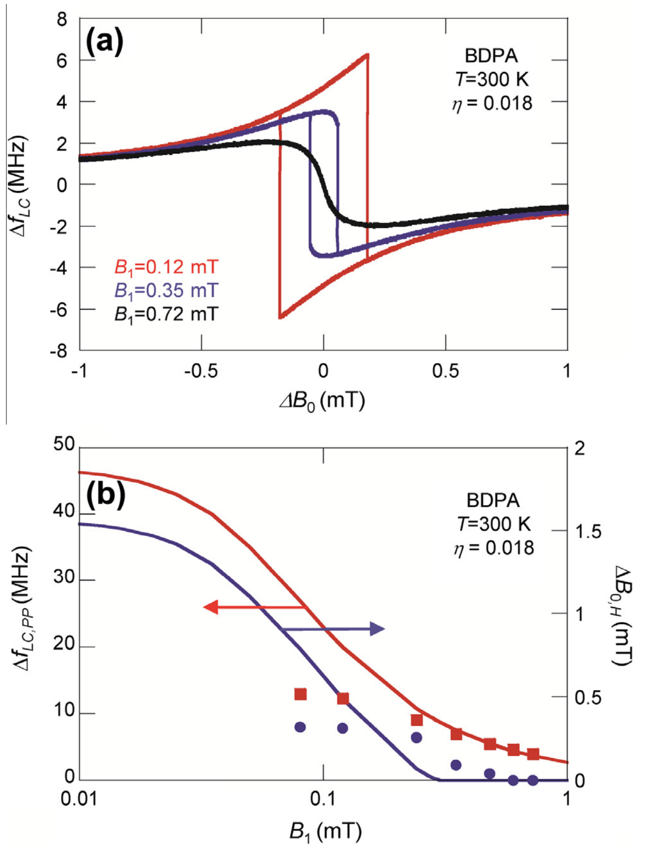

Fig. 5. Experiments and simulations with a sample of BDPA of about $60 \times 70 \times 30\ \mu m^3$ with $f_{LC} \cong 20.6$ GHz, $B_0 \cong 0.74$ T (for $\Delta B_0 = 0$). (a) Experimental oscillator frequency variation as a function of the static magnetic field for different values of B_1. (b) Oscillator frequency variation (red line: simulated values, red dots: experimental values) and hysteresis width (blue line: simulated values, blue dots: experimental values) as a function of B_1 (simulation parameters: $T_1 = T_2 = 100$ ns, $n = 1.5 \times 10^{27}$ spins/m^3, $\eta = 0.018$, $\gamma_e/2\pi = 28$ GHz/T). (For interpretation of the references to colour in this figure legend, the reader is referred to the web version of this article.)

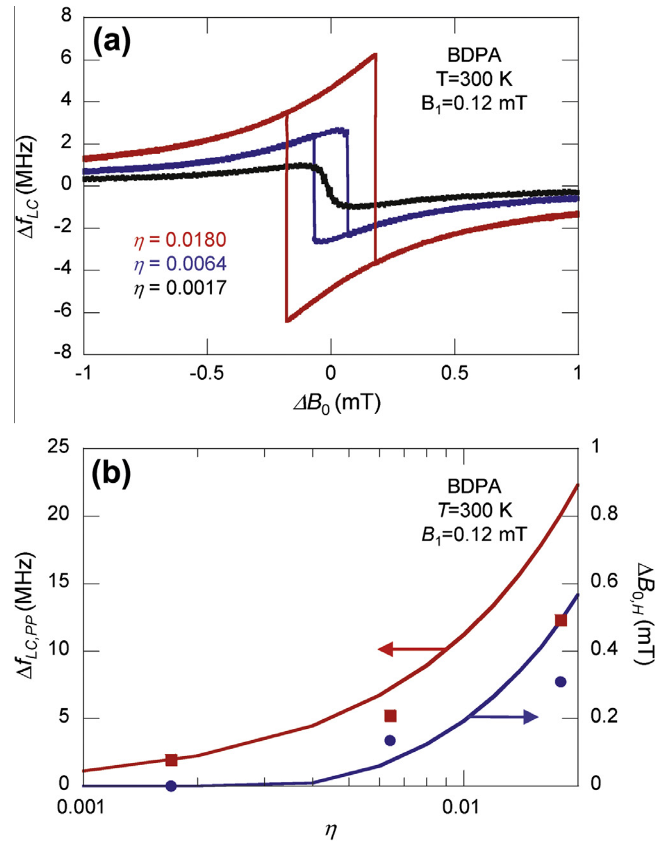

Fig. 6. Experiments and simulations with BDPA samples with $f_{LC} \cong 20.6$ GHz, $B_0 \cong 0.74$ T (for $\Delta B_0 = 0$). (a) Experimental oscillator frequency variation as a function of the static magnetic field for different values of η. (b) Oscillator frequency variation (red line: simulated values, red dots: experimental values) and hysteresis width (blue line: simulated values, blue dots: experimental values) as a function of η (simulation parameters: $T_1 = T_2 = 100$ ns, $n = 1.5 \times 10^{27}$ spins/m^3, $B_1 = 0.12$ mT, $\gamma_e/2\pi = 28$ GHz/T). (For interpretation of the references to colour in this figure legend, the reader is referred to the web version of this article.)

regime. Consequently, miniaturized integrated LC-oscillators appears to be a promising alternative approach to those currently used for the investigation of the strong coupling regime [1–5,8], potentially also with very small ensembles of spins at low temperature.

Acknowledgment

Financial support from the Swiss National Science Foundation is gratefully acknowledged.

Appendix A. Oscillation frequency of an LC-oscillator coupled with an ensemble of electron spins

Fig. A1a shows a general oscillator model. The admittance of the resonator and the negative admittance can be generically written as $Y = G + jB$ and $Y_{(-)} = G_{(-)} + jB_{(-)}$. An oscillator can sustain stable oscillations if $G_{(-)} + G = 0$ and $B_{(-)} + B = 0$ (see Ref. [26], p. 98). An LC-oscillator can be schematically represented, in first approximation, as in Fig. A1b, where we assume that the losses in the LC-resonator are mainly due to the coil series resistance R_L. The combination of the LC-resonator and the negative resistance $(-R)$ constitute the LC-oscillator. The negative resistance $(-R)$ compensate for the losses into the coil series resistance. If we consider that the oscillator is implemented as sketched in Fig. A1b we have

$$G = \frac{R_L}{R_L^2+\omega^2L^2}, \quad B = \frac{-\omega L}{R_L^2+\omega^2L^2} + \omega C, \qquad G_{(-)} = -\frac{1}{R}, \quad B_{(-)} = 0. \tag{A1}$$

From the condition $B = -B_{(-)} = 0$, we obtain a condition on the frequency ω. This corresponds to the oscillation frequency of the LC-oscillator with losses and it is given by

$$\omega_{LC,OSC} = \omega_{LC}\sqrt{1 - \frac{R_L^2 C}{L}}, \tag{A2}$$

where $\omega_{LC} = 1/\sqrt{LC}$ is the oscillation frequency of the LC-oscillator if the losses in the resonator are neglected. From the condition $G_{(-)} + G = 0$ we obtain a condition on the negative resistance value. At the oscillation frequency of the LC-oscillator (i.e., for $\omega = \omega_{LC,OSC}$) we obtain $R = Q^2 R_L$, where $Q \equiv \omega_{LC} L/R$ is the quality factor of the resonant circuit.

In a complementary-metal–oxide–semiconductor (CMOS) technology the negative resistance is often implemented with a cross-coupled pair of metal–oxide–semiconductor-field-effect-transistors (MOSFETs) as shown in Fig. A1c (see Ref. [27], p. 516). The admittance of the cross-coupled pair of transistors is $Y_{(-)} = -g_m/2$ where g_m is the transconductance of each of the two identical MOSFETs (see Ref. [27], p. 516). The transconductance g_m is a real positive quantity which depends, among others parameters, on the ratio width/length of the transistors, the carrier mobility,

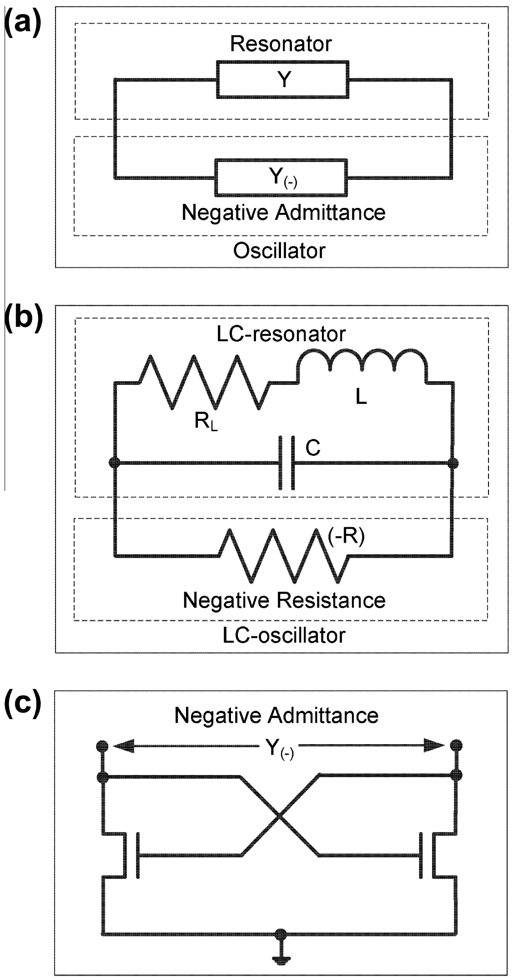

Fig. A1. (a) Schematic representation of a generic oscillator, (b) schematic representation of an LC-oscillator, (c) negative resistance realized with a cross-coupled pair of MOSFETs.

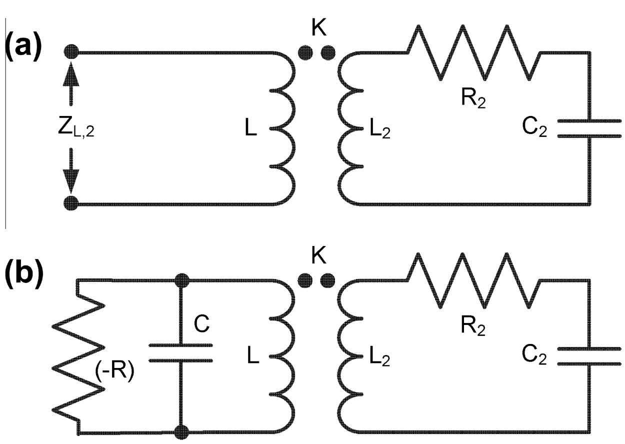

Fig. B1. (a) Equivalent electrical circuit for a coil coupled with a spin ensemble described by the Bloch equation with a non-saturating steady state excitation, (b) an LC-oscillator coupled with a LC-resonator.

and the gate oxide capacitance per unit of area (see Ref. [28], p. 91). The oscillation condition $R = Q^2R_L$ is, consequently, given by g_mR_L-$Q^2 = 2$. In practical circuits g_m must be larger than $(2/Q^2R_L)$ to sustain stable oscillation (see Ref. [27], p. 517).

The magnetization dynamics of an ensemble of spins can be described, in first approximation, by the Bloch phenomenological equation (see Ref. [29], p. 45). From the steady state solution of the Bloch equation, the complex susceptibility of a spin ensemble can be written as $\chi = \chi' - j\chi''$ where

$$\begin{aligned}\chi' &= -\frac{1}{2}\frac{\Delta\omega T_2^2}{1+(T_2\Delta\omega)^2+\gamma_e^2B_1^2T_1T_2}\omega_0\chi_0,\\ \chi'' &= \frac{1}{2}\frac{T_2}{1+(T_2\Delta\omega)^2+\gamma_e^2B_1^2T_1T_2}\omega_0\chi_0.\end{aligned} \tag{A3}$$

The impedance of a coil filled with a material having susceptibility χ is (see Ref. [29], p. 75 or Ref. [30], p. 37)

$$Z_\chi = j\omega L(1+\eta\chi) + R = j\omega L_\chi + R_\chi, \tag{A4}$$

where $L_\chi = L(1 + \eta\chi')$ and $R_\chi = R + \omega L\eta\chi''$. L and R are the inductance and the resistance of the coil without the sample, respectively. The filling factor η is given by

$$\eta = \left(\int_{V_s}|\mathbf{B}_u(\mathbf{x})|^2d\mathbf{x}^3 \Big/ \int_V |\mathbf{B}_u(\mathbf{x})|^2d\mathbf{x}^3\right) \cong (V_s/V_c), \tag{A5}$$

where V_s is the sample volume, V is the entire space, V_c is the sensitive volume of the coil, and $\mathbf{B}_u$ is the field produced by a unitary current in the coil (in T/A).

From Eq. (A2) we have, consequently, that the oscillation frequency of an LC-oscillator coupled with an ensemble of electron spins is given by

$$\omega_{LC,OSC,\chi} = \frac{1}{\sqrt{L_\chi C}}\sqrt{1-\frac{R_\chi^2C}{L_\chi}}. \tag{A6}$$

Since in most of the experimental conditions we have that $(R_\chi^2C/L_\chi) \ll 1$, we finally have

$$\omega_{LC,OSC,\chi} \cong \frac{1}{\sqrt{L_\chi C}} = \frac{\omega_{LC}}{\sqrt{1+\eta\chi'}}, \tag{A7}$$

which is the equation that we have used to compute the oscillation frequency of an LC-oscillator coupled with an ensemble of electron spins (i.e., Eq. (1) of the main text).

Appendix B. Frequency pulling for an LC-oscillator coupled with an ensemble of spins

Fig. B1a shows a circuit consisting of an inductor coupled with an LC-resonator with losses. The impedance of this circuit if given by

$$\begin{aligned}Z_{L,2} &= j\omega L\\ &+\frac{1}{2}\omega^2LK^2\left(\frac{2L_2/R_2}{1+f^2((L_2/R_2)\Delta\omega)^2} - j\frac{\Delta\omega(L_2/R_2)^22f}{1+f^2((L_2/R_2)\Delta\omega)^2}\right),\end{aligned} \tag{B1}$$

where $\omega_2 = 1/\sqrt{L_2C_2}$, $\Delta\omega = \omega - \omega_2$, $f = (2\omega_2 + \Delta\omega)/(\omega_2 + \Delta\omega)$. For $\Delta\omega \ll \omega_2$ we have that $f \cong 2$ and, consequently,

$$\begin{aligned}Z_{L,2} &\cong j\omega L\\ &+\frac{1}{2}\omega^2LK^2\left(\frac{2L_2/R_2}{1+((2L_2/R_2)\Delta\omega)^2} - j\frac{\Delta\omega(2L_2/R_2)^2}{1+((2L_2/R_2)\Delta\omega)^2}\right).\end{aligned} \tag{B2}$$

As shown in Appendix A, the impedance of a coil containing an ensemble of spins is

$$\begin{aligned}Z_\chi &= j\omega L_\chi + R_\chi\\ &= j\omega L\\ &+\frac{\omega^2L\eta\chi_0}{2}\left(\frac{T_2}{1+(T_2\Delta\omega)^2+\gamma_e^2B_1^2T_1T_2} - j\frac{\Delta\omega T_2^2}{1+(T_2\Delta\omega)^2+\gamma_e^2B_1^2T_1T_2}\right).\end{aligned} \tag{B3}$$

In condition of negligible saturation of the spin ensemble (i.e., for $\gamma_e^2B_1^2T_1T_2 \ll 1$) we have

$$Z_\chi \cong j\omega L_\chi + R_\chi = j\omega L + \frac{\omega^2 L\eta\chi_0}{2}\left(\frac{T_2}{1+(T_2\Delta\omega)^2} - j\frac{\Delta\omega T_2^2}{1+(T_2\Delta\omega)^2}\right). \quad \text{(B4)}$$

From the comparison of Eq. (B2) with Eq. (B4) we can state that a coil containing an ensemble of spins can be modelled by a coil coupled with an RLC series resonator with the following conditions:

$$\gamma_e B_0 = 1/\sqrt{L_2 C_2}, \quad T_2 = 2L_2/R_2, \quad \eta\chi_0 = K^2. \quad \text{(B5)}$$

Fig. B1b shows an LC-oscillator coupled with an LC-resonator. In this purely electrical coupled system the so-called frequency pulling phenomenon is observed if the inductive coupling between the oscillator and the resonator K is larger than a critical value $K_{cr} = R_2/\omega_2 L_2$ (see Ref. [26], p. 110). For a coupling stronger than the critical coupling the oscillation frequency of the oscillator–resonator system shows a hysteretic behaviour with sharp transitions with respect to a variation of the resonator frequency ω_2, the same behaviour that we observe in this work for a LC-oscillator coupled with a spin ensemble with respect to a variation of the magnetic field B_0 (which determines a variation of the spin ensemble resonance frequency $\omega_0 = \gamma B_0$). As shown above an ensemble of spins can be modelled by an LC-resonator coupled with a coil with a coupling factor $K^2 = \eta\chi_0$. The critical coupling is, hence, given by $K_{cr} = 2/T_2\omega_0$ and the condition $K \geqslant K_{cr}$ corresponds to $(\eta\chi_0)^{1/2}T_2\omega_0 \geqslant 2$. This is the condition that determines, in condition of negligible saturation, the onset of the hysteresis and the sharp transitions in the solution of Eq. (1). This condition is mathematically equivalent to the condition $g_c \cong \mu\sqrt{\mu_0\omega/2\hbar V_c}\sqrt{N_p} = \mu\sqrt{\mu_0\omega n_p\eta/2\hbar} \geqslant \gamma$ where $\gamma \cong 1/T_2$ and n_p is the density of polarized spins in the sample (in spins/m^3).

Appendix C. Oscillator linewidth compression

The effective half linewidth for an LC-oscillator and an LC-resonator are given by $\kappa \cong r(\omega/2Q)$ and $\kappa \cong \omega/2Q$, respectively [21]. For an LC-oscillator with phase noise dominated by the thermal noise of the LC-resonator circuit, the linewidth compression ratio r is given by $r = (1/V_0^2)(k_B T/C)$, where C is the LC-resonator capacitance, T is the temperature, Q is the LC-resonator quality factor, and V_0 is the oscillation voltage amplitude [21]. For $r \ll 1$ the active positive feedback in the oscillator allows to achieve more easily the strong coupling regime with respect to the corresponding resonator.

Appendix D. Sample preparation

The sample used in the measurements reported in Fig. 4 is a single crystal of 2,2-diphenyl-1-picrylhydrazyl (DPPH, Aldrich D9132), obtained by slow evaporation at room temperature in air of a solution of DPPH in ether (0.13% in volume of DPPH). The solution is placed in a 2 mL container closed with a cap having a hole of about 0.16 mm in diameter. With this procedure (similar to that reported in Ref. [31]) single crystal needles having dimensions of the order of $500 \times 200 \times 100\ \mu m^3$ are obtained in about 4 days. The use of single crystals instead of grains is not essential but it helps for a more precise evaluation of the sample volume (we observed hysteresis and sharp transitions also with DPPH grains as received from Aldrich). The value of T_2 for the obtained crystals, evaluated from linewidth measurements at low B_1 using a conventional electron spin resonance spectrometer, is 56 ± 4 ns at 300 K as well as 77 K.

The sample used in the measurements reported in Figs. 5 and 6 are particles of 1:1 α,γ-bisdiphenylene-β-phenylallyl/benzene complex (BDPA with benzene, Aldrich 152560) without any further treatment.

Appendix E. Comparison between theoretical and experimental results

As shown in Figs. 4d, 5b, and 6b the experimental results for the frequency variation $\Delta f_{LC,PP}$ and the hysteresis width $\Delta B_{0,H}$ are up to a factor four smaller than the values obtained by solving Eq. (1) with the parameters given in the figure caption. The agreement improves only marginally by considering that the B_1 amplitude and direction is non-uniform over the sample volume. The difference between the experimental and simulated results is probably due to the uncertainty on the values of T_1, B_1, spin density, and sample volume. The relaxation time T_1 for DPPH varies by an order of magnitude depending on the solvent in which the samples are crystallized [32–35]. This, in turn, influences also the estimation of B_1 by linewidth broadening experiments. The spin density value for DPPH reported in the literature varies by about 50%, from 1.5×10^{27} to 2.3×10^{27} spins/m^3 [18,31,32]. The spin density and relaxation times for the BDPA sample used in the simulations (i.e., $n = 1.5 \times 10^{27}$ spins/m^3 and $T_1 = T_2 = 100$ ns) are, respectively, obtained from the density value of 1220 kg/m^3 as reported in Ref. [36], and the relaxation time values as reported in Ref. [35,37]. For both samples, the error in the estimation of their volume is in the order of ±30%. Several sets of reasonable values for these parameters (i.e., T_1, T_2, B_1, spin density, and sample volume) can produce simulation results that fit the experimental results within a factor of two, although none is capable to produce a better agreement. This might be due to the *intrinsic* fact that Eq. (1) is obtained assuming that the Bloch equation is valid and that the LC-oscillator frequency is given by Eq. (A2). Nevertheless, the simple theory proposed here describes, at least semi-quantitatively, the phenomena observed in this work. An interesting future work might be the theoretical and experimental investigation of the strong coupling regime using our LC-oscillator approach with ensemble of spins where the Bloch equation (and, consequently, Eq. (1)) is not applicable and a quantum mechanical approach might be required to describe the spin ensemble behaviour.

Appendix F. Spin sensitivity and strong coupling at low temperatures

In Refs. [19,20] we derived the following equation for the spin sensitivity (in spins/Hz$^{1/2}$)

$$N_{\min} \cong \alpha\frac{T^{3/2}\sqrt{R}}{B_0^2 B_u}\sqrt{\frac{T_1}{T_2}}, \quad \text{(F1)}$$

where R is the coil series resistance, B_u is the coil unitary field, T is the coil (and sample) temperature, and $\alpha \cong 20\ m^{-1}\ kg^{5/2}\ s^{-4}\ K^{-3/2}\ A^{-3}$. Assuming $T = 1$ K, $T_1 = T_2 = 10\ \mu s$, $R = 1\ \Omega$, $f_{LC} = 280$ GHz, $B_u = 0.13$ T/A (i.e., a single turn coil with a diameter of 10 μm), and $\kappa \cong 10^4$ rad/s, we obtain $N_{\min} \cong 1$ spin/Hz$^{1/2}$, $\gamma \cong 10^5$ rad/s, and, for a single spin, $g_c \cong 10^5$ rad/s. Under these assumptions the spin sensitivity and the coupling parameters are at the limit of allowing the detection of a single spin in the strong coupling regime. Here we discuss these assumptions in some details:

(1) $T = 1$ K: Despite of impurity freeze-out problems, several CMOS integrated circuits have shown to be still operative down to 4 K at least [38–40].

(2) $T_1 \cong T_2 \cong 10\ \mu s$: T_1 is often much longer than T_2 at low temperatures. Moreover, relaxation times of 10 μs require $B_1 < 1\ \mu T$ to avoid significant saturation, and, consequently,

microwave currents below 10 μA for a 10 μm diameter single turn coil. This would in turn require bias currents in the oscillator which can hardly produce a sufficiently large transconductance in the MOS transistors to sustain stable oscillations, at least with the oscillator topology that we are currently using [27]. This is certainly the most critical assumption and will require careful design of the oscillator topology.

(3) $R = 1\ \Omega$: A single turn coil having a diameter of 10 μm, a wire width of 1 μm, a conservative impurity limited resistivity $\rho_{1K} \cong (1/10)\rho_{300K} \cong 2 \times 10^{-9}\ \Omega$ m, and a skin depth limited effective thickness of $t = 80$ nm, will have a resistance $R_{1K,280GHz} \cong 0.8\ \Omega$.

(4) $f_{LC} = 280$ GHz: Operation at 280 GHz should also be feasible (a 300 GHz integrated silicon LC-oscillator has been recently demonstrated [41]).

(5) $\kappa \cong 10^4$ rad/s: The assumption of an oscillator linewidth $\kappa \cong 10^4$ rad/s at 1 K and 280 GHz (i.e., similar to the value reported in this paper at 300 K and 20 GHz) is realistic (the oscillator linewidth is proportional to the frequency noise spectral density which, in turn, is proportional to $\omega_{LC}^2 T$ [20]).

References

[1] Y. Kubo, I. Diniz, A. Dewes, V. Jacques, A. Dreau, J.F. Roch, A. Auffeves, D. Vion, D. Esteve, P. Bertet, Storage and retrieval of a microwave field in a spin ensemble, Phys. Rev. A 85 (2012) 012333.

[2] E. Abe, H. Wu, A. Ardavan, J.J.L. Morton, Electron spin ensemble strongly coupled to a three-dimensional microwave cavity, Appl. Phys. Lett. 98 (2011) 251108.

[3] X.B. Zhu, S. Saito, A. Kemp, K. Kakuyanagi, S. Karimoto, H. Nakano, W.J. Munro, Y. Tokura, M.S. Everitt, K. Nemoto, M. Kasu, N. Mizuochi, K. Semba, Coherent coupling of a superconducting flux qubit to an electron spin ensemble in diamond, Nature 478 (2011) 221–224.

[4] Y. Kubo, F.R. Ong, P. Bertet, D. Vion, V. Jacques, D. Zheng, A. Dreau, J.F. Roch, A. Auffeves, F. Jelezko, J. Wrachtrup, M.F. Barthe, P. Bergonzo, D. Esteve, Strong coupling of a spin ensemble to a superconducting resonator, Phys. Rev. Lett. 105 (2010) 140502.

[5] D.I. Schuster, A.P. Sears, E. Ginossar, L. DiCarlo, L. Frunzio, J.J.L. Morton, H. Wu, G.A.D. Briggs, B.B. Buckley, D.D. Awschalom, R.J. Schoelkopf, High-cooperativity coupling of electron-spin ensembles to superconducting cavities, Phys. Rev. Lett. 105 (2010) 140501.

[6] J.H. Wesenberg, A. Ardavan, G.A.D. Briggs, J.J.L. Morton, R.J. Schoelkopf, D.I. Schuster, K. Molmer, Quantum computing with an electron spin ensemble, Phys. Rev. Lett. 103 (2009) 070502.

[7] A. Imamoglu, Cavity QED based on collective magnetic dipole coupling: spin ensembles as hybrid two-level systems, Phys. Rev. Lett. 102 (2009) 083602.

[8] P. Bushev, A.K. Feofanov, H. Rotzinger, I. Protopopov, J.H. Cole, C.M. Wilson, G. Fischer, A. Lukashenko, A.V. Ustinov, Ultralow-power spectroscopy of a rare-earth spin ensemble using a superconducting resonator, Phys. Rev. B 84 (2011) 060501.

[9] R. Amsuss, C. Koller, T. Nobauer, S. Putz, S. Rotter, K. Sandner, S. Schneider, M. Schrambock, G. Steinhauser, H. Ritsch, J. Schmiedmayer, J. Majer, Cavity QED with magnetically coupled collective spin states, Phys. Rev. Lett. 107 (2011) 060502.

[10] S. Bertaina, N. Groll, L. Chen, I. Chiorescu, Tunable multiphoton Rabi oscillations in an electronic spin system, Phys. Rev. B 84 (2011) 134433.

[11] I. Chiorescu, N. Groll, S. Bertaina, T. Mori, S. Miyashita, Magnetic strong coupling in a spin-photon system and transition to classical regime, Phys. Rev. B 82 (2010) 024413.

[12] S. Miyashita, T. Shirai, T. Mori, H. De Raedt, S. Bertaina, I. Chiorescu, Photon and spin dependence of the resonance line shape in the strong coupling regime, J. Phys. B 45 (2012) 124010.

[13] Y. Kubo, C. Grezes, A. Dewes, T. Umeda, J. Isoya, H. Sumiya, N. Morishita, H. Abe, S. Onoda, T. Ohshima, V. Jacques, A. Dreau, J.F. Roch, I. Diniz, A. Auffeves, D. Vion, D. Esteve, P. Bertet, Hybrid quantum circuit with a superconducting qubit coupled to a spin ensemble, Phys. Rev. Lett. 107 (2011) 220501.

[14] S. Bertaina, L. Chen, N. Groll, J. Van Tol, N.S. Dalal, I. Chiorescu, Multiphoton coherent manipulation in large-spin qubits, Phys. Rev. Lett. 102 (2009) 050501.

[15] O.W.B. Benningshof, H.R. Mohebbi, I.A.J. Taminiau, G.X. Miao, D.G. Cory, Superconducting microstrip resonator for pulsed ESR of thin films, J. Magn. Reson. 230 (2013) 84–87.

[16] F. Beuneu, Unusual behaviour of a very narrow electron spin resonance signal, J. Magn. Reson. 227 (2013) 46–50.

[17] N. Bloembergen, S. Wang, Relaxation effects in para-magnetic and ferromagnetic resonance, Phys. Rev. 93 (1954) 72–83.

[18] R. Griffiths, Theory of magnetic exchange-lattice relaxation in 2 organic free radicals, Phys. Rev. 124 (1961) 1023–1030.

[19] T. Yalcin, G. Boero, Single-chip detector for electron spin resonance spectroscopy, Rev. Sci. Instrum. 79 (2008) 094105.

[20] J. Anders, A. Angerhofer, G. Boero, K-band single chip electron spin resonance detector, J. Magn. Reson. 217 (2012) 19–26.

[21] D. Ham, A. Hajimiri, Virtual damping and Einstein relation in oscillators, IEEE J. Solid-State Circuits 38 (2003) 407–418.

[22] A. Bevilacqua, P. Andreani, An analysis of 1/f noise to phase noise conversion in CMOS harmonic oscillators, IEEE Trans. Circ. Syst. 59 (2012) 938–945.

[23] A.M. Tyryshkin, S. Tojo, J.J.L. Morton, H. Riemann, N.V. Abrosimov, P. Becker, H.J. Pohl, T. Schenkel, M.L.W. Thewalt, K.M. Itoh, S.A. Lyon, Electron spin coherence exceeding seconds in high-purity silicon, Nat. Mater. 11 (2012) 143–147.

[24] C.D. Weis, C.C. Lo, V. Lang, A.M. Tyryshkin, R.E. George, K.M. Yu, J. Bokor, S.A. Lyon, J.J.L. Morton, T. Schenkel, Electrical activation and electron spin resonance measurements of implanted bismuth in isotopically enriched silicon-28, Appl. Phys. Lett. 100 (2012).

[25] J.J.L. Morton, D.R. McCamey, M.A. Eriksson, S.A. Lyon, Embracing the quantum limit in silicon computing, Nature 479 (2011) 345–353.

[26] J. Groszkowski, Frequency of Self-Oscillations, Pergamon Press, Oxford, 1964.

[27] B. Razavi, RF Microelectronics, second ed., Prentice Hall, Upper Saddle River, NJ, 2011.

[28] S.M. Sze, Semiconductor Devices Physics and Technology, second ed., Wiley, New York, 2002.

[29] A. Abragam, Principles of Nuclear Magnetism, reprinted ed., Clarendon Press, Oxford, 1994.

[30] C.P. Slichter, Principles of Magnetic Resonance, third enlarged and updated ed., Springer, Berlin, 1996.

[31] D. Zilic, D. Pajic, M. Juric, K. Molcanov, B. Rakvin, P. Planinic, K. Zadro, Single crystals of DPPH grown from diethyl ether and carbon disulfide solutions – crystal structures, IR, EPR and magnetization studies, J. Magn. Reson. 207 (2010) 34–41.

[32] G. Höcherl, H.C. Wolf, Zur Konzentrationsabhängigkeit der Elektronenspin-Relaxationszeiten von Diphenyl-Picryl-Hydrazyl in fester phase, Z. Phys. 183 (1965) 341–351.

[33] Krishnaji, B.N. Misra, Electron spin resonance absorption in recrystallized free radicals at low fields, J. Chem. Phys. 41 (1964) 1027–1033.

[34] Krishnaji, B.N. Misra, Spin–lattice relaxation in free-radical complexes, Phys. Rev. A – Gen. Phys. 135 (1964) 1068.

[35] J.P. Goldsborough, M. Mandel, G.E. Pake, Influence of exchange interaction on paramagnetic relaxation times, Phys. Rev. Lett. 4 (1960) 13–15.

[36] N. Azuma, T. Ozawa, J. Yamauchi, Molecular and crystal-structures of complexes of stable free-radical BDPA with benzene and acetone, Bull. Chem. Soc. Jpn. 67 (1994) 31–38.

[37] D.G. Mitchell, R.W. Quine, M. Tseitlin, R.T. Weber, V. Meyer, A. Avery, S.S. Eaton, G.R. Eaton, Electron spin relaxation and heterogeneity of the 1:1 alpha, gamma-Bisdiphenylene-beta-phenylallyl (BDPA)/benzene complex, J. Phys. Chem. B 115 (2011) 7986–7990.

[38] G. Ghibaudo, F. Balestra, Low temperature characterization of silicon CMOS devices, Microelectron. Reliab. 37 (1997) 1353–1366.

[39] B. Okcan, G. Gielen, C. Van Hoof, A third-order complementary metal–oxide–semiconductor sigma-delta modulator operating between 4.2 K and 300 K, Rev. Sci. Instrum. 83 (2012) 024708.

[40] H. Nagata, H. Shibai, T. Hirao, T. Watabe, M. Noda, Y. Hibi, M. Kawada, I. Nakagawa, Cryogenic capacitive transimpedance amplifier for astronomical infrared detectors, IEEE Trans. Electron Devices 51 (2004) 270–278.

[41] B. Razavi, A 300-GHz fundamental oscillator in 65-nm CMOS technology, IEEE J. Solid-State Circuits 46 (2011) 894–903.